Applied Thermal Engineering 230 (2023) 120753

Contents lists available at ScienceDirect

Applied Thermal Engineering

journal homepage: www.elsevier.com/locate/apthermeng

Research Paper

Challenges and feasibility of a six-stroke engine using water direct injection

Yubeen Yang [a], Hoseung Yi [a], Seungho Yang [a], Sungwook Park [b,*]

[a] Department of Mechanical Convergence Engineering, Hanyang University Graduate School, Seoul 04763, Republic of Korea
[b] School of Mechanical Engineering, Hanyang University, Seoul 04763, Republic of Korea

ARTICLE INFO

Keywords:
Six-stroke engine
DISI engine
Water injection
Exhaust heat recovery
Steam expansion
Steam injection

ABSTRACT

As fuel efficiency and exhaust regulations have become more stringent, many studies have been conducted to improve fuel efficiency. One interesting proposal is to develop a six-stroke engine using water injection. However, there is a lack of research on this concept, and existing studies have only taken a theoretical approach or did not involve comparisons with a four-stroke engine, obscuring the feasibility of a six-stroke engine using water injection. So, in this study, we performed experiments and simulations of a six-stroke engine using water injection and compared the results with those of a four-stroke engine. We optimized the exhaust valve lift profile through simulation for an actual exhaust cam of the six-stroke engine, and modified a four-stroke port fuel injection engine to a six-stroke engine. Then, through experiments and simulations, we evaluated the feasibility and the challenges of building a six-stroke engine using water injection. We used the CONVERGE v2.4 software application and validated the simulation models through the results of experiments. Using these models, we conducted simulations with various injection timings, masses, and water temperatures. The results indicate that the cylinder wall is cooled due to continuous water injection making evaporation unstable and that wall-temperature control is required in order to realize a six-stroke engine using water injection. In a simulation assuming the constant temperature of the wall, as additional strokes are added, the indicated mean effective pressure (IMEP) decreases by about 0.4 bar compared to that of the four-stroke engine, and only about 40% of this loss is recovered through water injection. The wall evaporation ratio is more critical to the feasibility of the six-stroke engine using water injection than other parameters. We show that it is very difficult to achieve a six-stroke engine using water injection unless a significant amount of heat energy for evaporation is brought from sources other than the mixture in the cylinder. The challenges of a six-stroke engine using water injection were cylinder temperature control and latent heat of water. If excessive cooling does not occur, such as in steam injection, IMEP can increase due to an increase in mass. However, this is very ideal case. It is difficult to obtain energy elsewhere for evaporation, and due to the latent heat of water, the mixture is inevitably cooled down making it difficult to realize this concept of six-stroke engine.

1. Introduction

With regulations related to the efficiency of the engine and emissions becoming stringent due to environmental problems, extensive research has been conducted to increase the efficiency of engines [1–5]. The efficiency of an engine can be increased by enhancing the combustion efficiency and reducing the wasted energy. First, the primary way to maximize the combustion efficiency is to induce the fuel and air to react well, resulting in almost complete combustion. For this, extensive research has been conducted to attempt strategies such as multi-stage injection [6,7] or lean combustion [8,9]. Meanwhile, the recoverable wasted energy includes friction loss, exhaust loss, and cooling loss. These losses can be reduced to increase the efficiency of the engine. For example, studies have been conducted to reduce friction in the piston [10,11] or cam systems [12,13] by changing the shapes or characteristics of surfaces. In addition, studies have been conducted to adjust valve variables to minimize the energy that could not be converted to work due to fixed valve variables [14–16]. As such, numerous studies have

Abbreviations: ASOE, after start of energizing; ATDC, after top dead center; BDC, bottom dead center; BTDC, before top dead center; CA, crank angle; DI, direct injection; EVC, exhaust valve closed; EVO, exhaust valve open; GDI, gasoline direct injection; IMEP, indicated mean effective pressure; IVC, intake valve closed; IVO, intake valve open; KH, Kelvin–Helmholtz; PFI, port fuel injection; RT, Rayleigh–Taylor; TDC, top dead center; TKE, turbulence kinetic energy; LPM, liter per mean.

* Corresponding author.
E-mail address: parks@hanyang.ac.kr (S. Park).

https://doi.org/10.1016/j.applthermaleng.2023.120753
Received 26 December 2022; Received in revised form 3 April 2023; Accepted 8 May 2023
Available online 12 May 2023

been conducted on the basis of existing engine systems. As a result, the improvement of engine efficiencies has dramatically slowed. To satisfy increasingly strong regulations, a new fuel-efficient paradigm is needed outside the existing four-stroke engine system.

One of these paradigms is a six-stroke engine using direct water injection. The six-stroke engine using direct water injection is a system that focuses on the wasted energy by enhancing the engine efficiency, as shown in Fig. 1. Conklin et al. [17] first suggested this system. To enhance the four-stroke engine, they added two additional strokes, partial exhaust (re-compression) and steam expansion strokes, between the power stroke and exhaust stroke. In this engine, water is heated using coolant, and this water is injected at the end of re-compression stroke to recover energy from the coolant and exhaust gas. To evaluate the feasibility of this system, they conducted a theoretical analysis of the additional strokes. In their analysis, the mean effective pressure (MEP) of additional strokes was calculated from 0.7 to 2.5 bar in accordance with the mass of water and the exhaust valve close timing. However, these calculations were conducted through a simple thermodynamic cycle analysis. Also, it was assumed that the water injection and evaporation were instantaneous, and heat transfer through the cylinder wall was neglected.

Meanwhile, Arabaci et al. [18] conducted an experimental study on the effect of water injection parameters on the six-stroke engine. They converted a single cylinder four-stroke gasoline engine into a six-stroke gasoline engine. In the stoichiometric condition, water injection was performed with various injection pressures and timings. Water injection reduced emissions such as CO, HC, and NO compared to the case without water injection. Also, the thermal efficiency increased by about 8.72%. However, they compared the results of the six-stroke engine with those of a six-stroke engine that did not spray water, not a four-stroke engine. Also, they used the engine mainly used for small generators. Furthermore, specific data, such as P-V diagram, were not provided. Thus, it could not be judged whether the six-stroke engine with water injection was more efficient than the four-stroke engine.

As such, there are no studies evaluating the specific feasibility of this six-stroke engine, and previous studies on six-stroke engines using direct water injection are insufficient. Thus, it is necessary to first evaluate the six-stroke engine using water injection. Therefore, in this study, the feasibility of a six-stroke engine using direct water injection was evaluated numerically by comparing the four-stroke engine and the six-stroke engine and verified through experiments. Then, challenges that affected the construction of the six-stroke engine were identified. The six-stroke engine system was modified by adding direct water injection process and two additional strokes, partial exhaust and steam expansion strokes, to the conventional four-stroke port-fuel-injection (PFI) gasoline engine. Computational fluid dynamics (CFD) was utilized for numerical analysis. Theoretical analysis was also performed. With four-stroke and six-stroke engines of the same configuration, experiments were performed for validation.

2. Methods

2.1. Mechanism of the six-stroke engine using water injection

The six-stroke engine using water injection recovers exhaust heat by evaporating water. For this engine, the six-stroke was constructed by adding a two-stroke cycle to the existing four-strokes. The mechanism of this engine is shown in Fig. 2.

In the six-stroke engine, the intake stroke to combustion expansion stroke were the same as in the four-stroke engine. Then, instead of an exhaust stroke, a partial exhaust (re-compression) stroke and steam expansion stroke continued. Finally, the exhaust stroke is carried out, and the entire process of the six-stroke engine is completed. In other words, there are two additional strokes between the combustion expansion stroke and exhaust stroke, compared to the four-stroke engine. Theoretically, this engine obtains additional work from the expansion force of steam generated by water injection at the end of the partial exhaust (re-compression) stroke. This process of obtaining additional work is shown in Fig. 3.

All of the processes, except the additional strokes, are the same as the four-stroke engine on the P-V diagram. Thus, additional work is obtained from positive work in the additional two strokes. Meanwhile, to realize the six-stroke engine, it is necessary to modify the actual cam shape as shown in Fig. 4.

Unlike the existing four-stroke engine cam, the six-stroke engine cam was designed to have a shape that allowed each stroke to occupy 60°.

2.2. Experimental apparatus and conditions

Spray visualization was conducted for validation of the spray breakup model. Distilled water with high purity was used in the spray experiment. Since water has the property of oxidizing iron, the fuel supply line was made of stainless steel (SUS304), which is not easily corroded. Also, the fuel accumulator was made of the same material due to corrosion. The limit pressure of the accumulator was 1,000 bar or more. The accumulator was designed to have a capacity of 0.5 L to reduce the fluctuation of the pressure. A Haskel pump (HSF-300) was used to supply high pressure into the fuel accumulator. A solenoid-type six-hole injector was used in the experiment. The details of experimental conditions are shown in Table 1.

For spray visualization, the Mie-scattering method was used. The Mie-scattering method is a visualization method utilizing the light scattered by the droplets. Two metal halogenated lamps (HCL4015) were used to irradiate light to the left and right sides of the spray. Spray visualization images were obtained using a high-speed camera (Phantom VEO 1310, 10,000 fps, 960x960, macro-focal 105 mm lens). 50 images per each experimental condition were acquired through injector control and synchronization with the high-speed camera using CompactRIO (National Instruments). Using MATLAB, the acquired images were overlapped and post-processed to create an average image. Then, the images were binarized based on the brightness, determining the

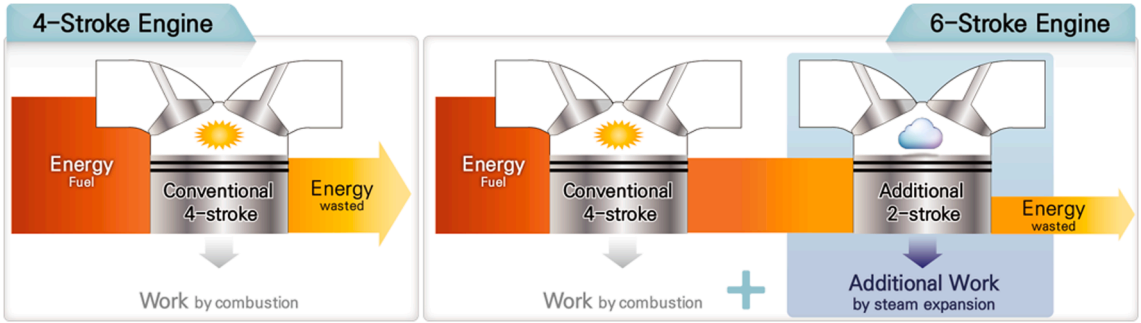

Fig. 1. Concept of the six-stroke engine using water injection.

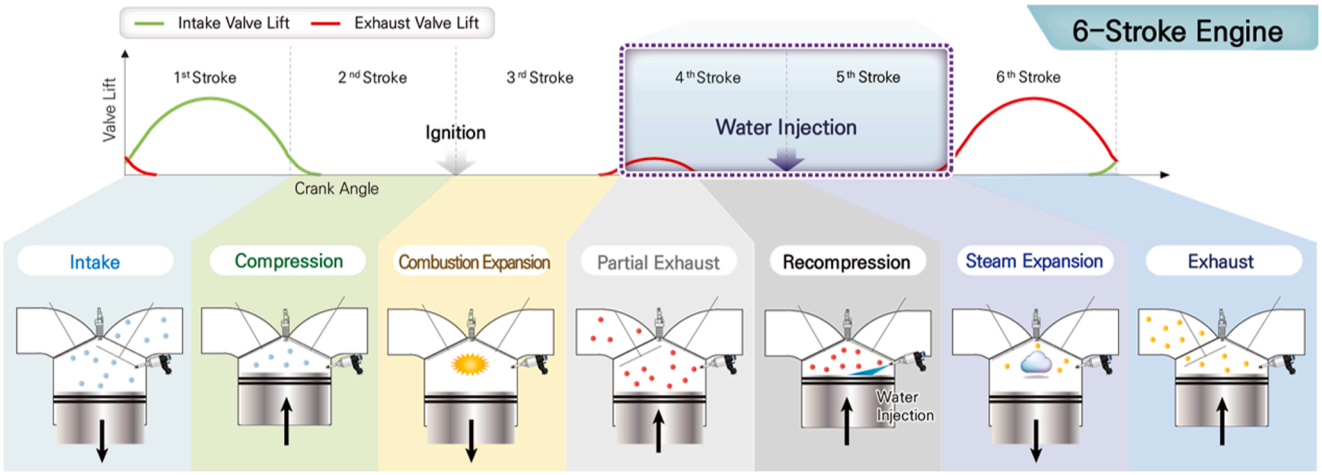

Fig. 2. Mechanism of the six-stroke engine using water injection.

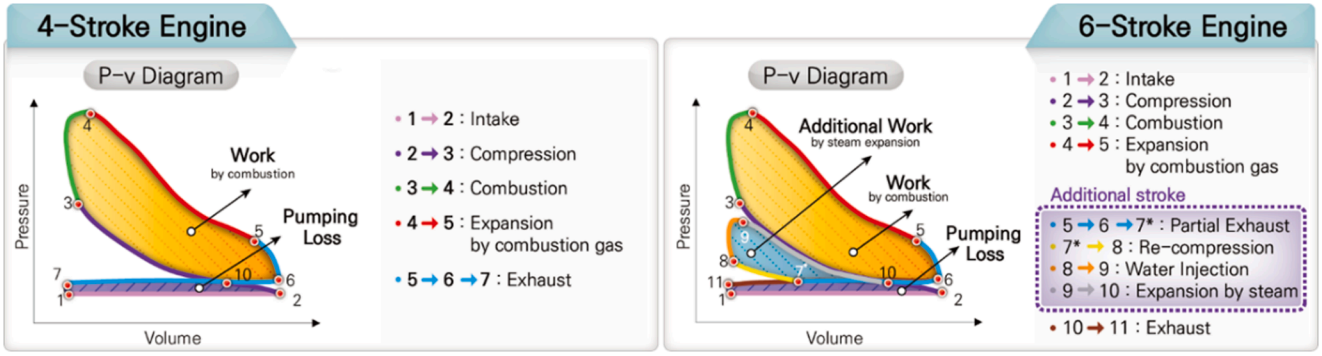

Fig. 3. Schematic of the six-stroke engine on a P-V diagram.

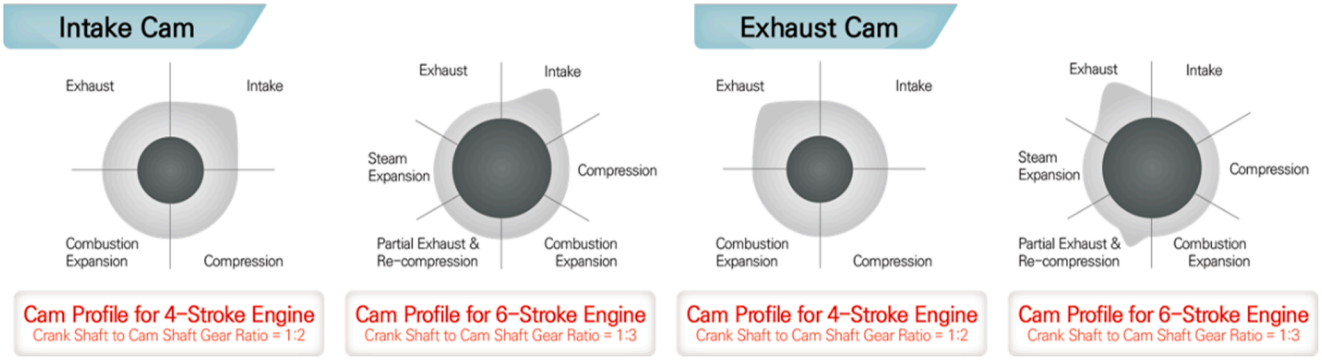

Fig. 4. Modification of the cam profile from the four-stroke engine into a six-stroke engine.

Table 1
Experimental conditions for the spray experiment.

Injector type	Solenoid-driven type, six holes
Test fluid	Distilled water (H_2O)
Fluid temperature [°C]	20
Injection pressure, P_{inj} [bar]	100, 200, 350
Injection duration [ms]	2
Ambient temperature [°C]	20
Ambient pressure [bar]	1

spray boundary. Last, the spray tip penetration was measured based on this boundary. The single-cylinder gasoline direct injection spark ignition (DISI) engine was modified to inject gasoline through the intake manifold using the conventional port fuel injector and inject water directly into the combustion chamber using a conventional high-flux wall-guided gasoline direct injector. The spark plug of this engine was oriented at the center of the cylinder head. The intake and exhaust camshafts for the six-stroke engine were designed by the following methods. Obtained by reverse engineering the four-stroke engine and calculated from simulation respectively, the valvetrain system parameters and valve lift of the six-stroke engine were implemented into VTDESIGN (Gamma Technologies) software to calculate the intake and exhaust cam lift of the six-stroke engine. Then, the calculated cam lift was provided to a camshaft manufacturer to precisely machine the intake and exhaust camshaft for the six-stroke engine. Detailed specifications of the engine are listed in Table 2.

Table 2
Six-stroke engine specifications.

Bore × stroke [mm]		76.98 × 85.44	
Compression ratio		10.5:1	
Displacement Volume [cc]		397.66	
Crankshaft/Camshaft gear ratio		3:1	
Intake valve lift [mm]		9.93	
Partial exhaust valve lift [mm]		5.05	
Full exhaust valve lift [mm]		8.13	
4-Stroke	**Valve timing [CA °]**	IVO	375
		IVC	625
		EVO	108
		EVC	346
Additional 2-Stroke	**Valve timing [CA °]**	EVO	828
		EVC	1008

CA 720°: TDC just before the combustion expansion stroke.

The engine was operated using an alternating current (AC) motor to maintain constant rotational speed. The intake air flow was provided using compressed dry air and maintained at a constant rate using a mass air flow controller and chamber. The fuel was constantly pressurized using a siphon fuel accumulator and nitrogen gas cylinder. The water was pressurized using an air-driven liquid pump while maintaining a pressure variance below 5 bar by using the fuel accumulator. The water temperature was elevated by the engine heat and a high-temperature band heater (Global Lab) wrapped injection rail and maintained by a GLTC-DP heat controller (Global Lab). The injection timing and spark timing were controlled using the CompactRIO (National Instruments) system hardware and LabVIEW (National Instruments) software. The injection duration was also controlled by CompactRIO and LabVIEW with feedback from an LSU 4.9 (Bosch) lambda sensor to maintain a constant equivalence ratio. Lambda sensor's accuracy at lambda 1 is 1.016 ± 0.007. The in-cylinder pressure was measured by a piezo electric pressure sensor integrated 6115B spark plug (Kistler) which was amplified by a 5064C11 charge amplifier (Kistler) and data were acquired with a USB-6341 multifunction I/O device (National Instruments). Kistler 611B piezo electric pressure sensor integrated spark plug has a sensitivity of −10 pC/bar at 200 °C. 99 cycles of in-cylinder pressure were measured, then, the average and variance were calculated to minimize cyclic variation and to check for combustion instability. The in-cylinder average pressure and volume relating to the crank angle were post-processed to calculate the heat release rate (HRR), total heat release (THR), and IMEP. The details of the positions and wiring of the system explained above are illustrated in Fig. 5 and an image of the engine is shown in Fig. 6.

The six-stroke engine rotation speed and coolant temperature were maintained at 1500 rpm and 90 °C, respectively. The intake air flow rate was maintained at 87 LPM, which is equivalent to a medium load throttle for the six-stroke engine. The equivalence ratio was set to be stoichiometric by the controlling PFI injection duration and the spark timing was set to be at the maximum brake torque (MBT) for all cases. The PFI injection pressure was maintained at 5 bar and the end of injection (EOI) timing was maintained at BTDC 330°. 10 mg of water was injected by controlling the injection duration of the GDI injector. The GDI injection pressure was set to 350 bar and the injection timing was set from ATDC 340° to ATDC 360°. The water temperature was set to be maintained at about 90 °C. Distilled water was used to reduce the corrosion of the combustion chamber. The test conditions listed above are summarized in Table 3.

2.3. Computational methodology and conditions

2.3.1. Computational models

In this study, the CONVERGE v2.4 software was used. The RNG k-ε model [19] was used to simulate turbulent flow. Unlike the standard k-ε

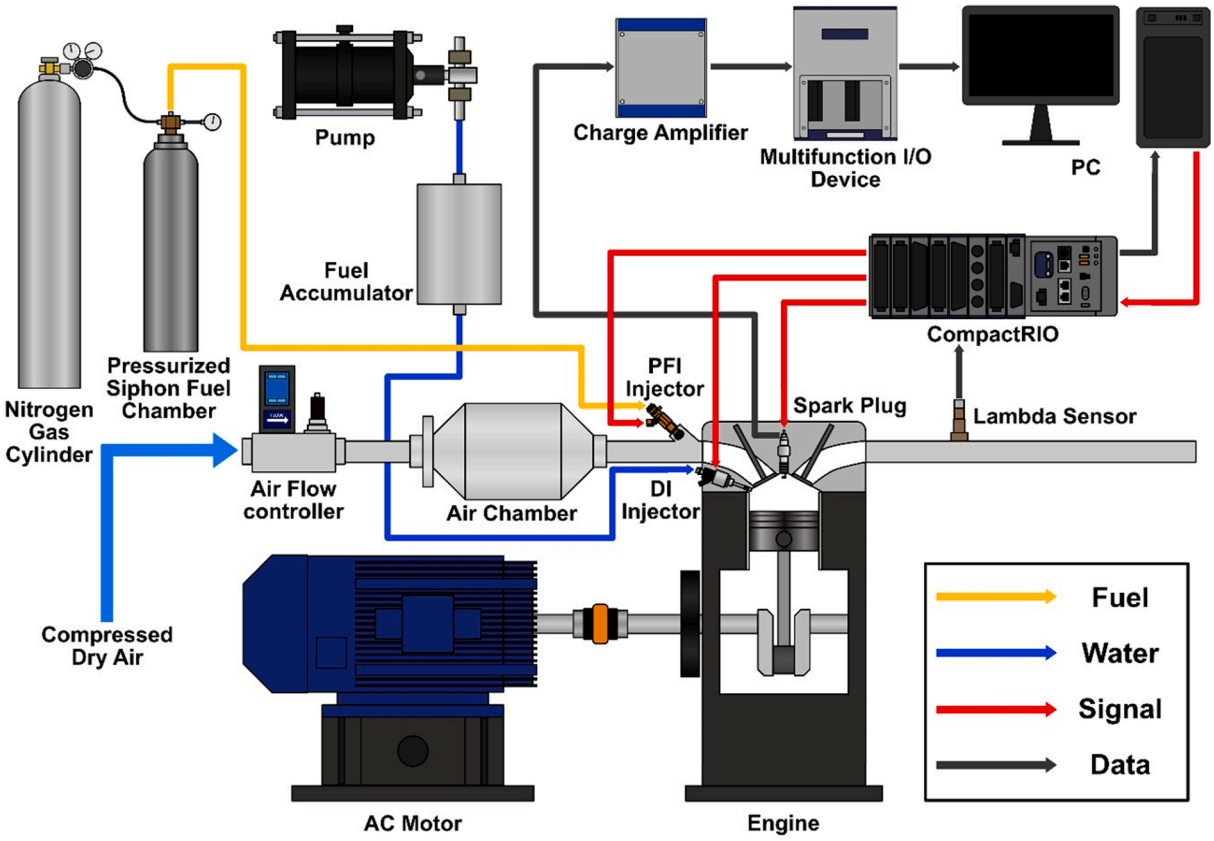

Fig. 5. Schematic of the six-stroke single-cylinder engine operating and measurement system.

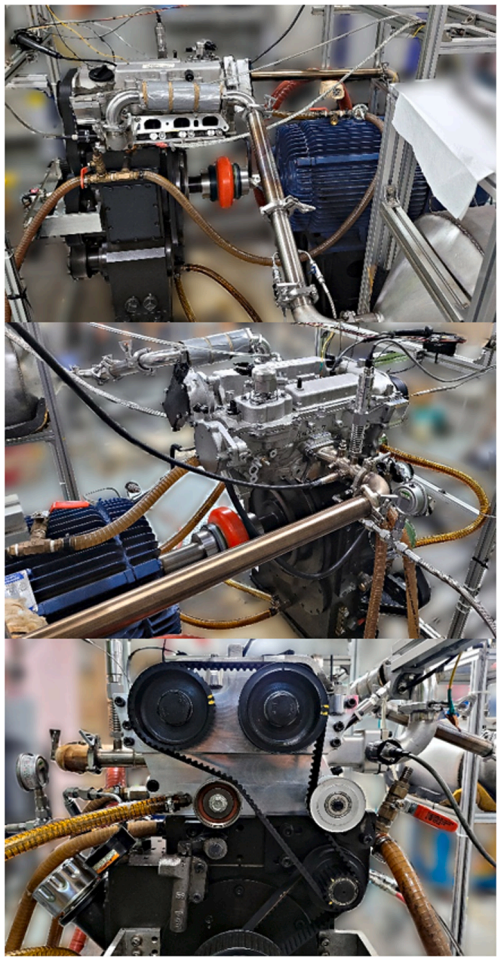

Fig. 6. Image of the six-stroke single cylinder engine.

Table 3
Six-stroke engine operating conditions.

Engine speed [rpm]	1500
Coolant temperature [°C]	90
Intake air flow rate [LPM]	87
Equivalence ratio	1.0
Spark timing	MBT
PFI injection pressure [bar]	5
PFI end of injection (EOI) [° BTDC]	330
Water injection mass [mg]	10
Water temperature [°C]	90
DI injection pressure [bar]	350
DI injection timing [° ATDC]	340 ~ 380

TDC: just before the combustion expansion stroke.

model, this model has a modified form of the epsilon equation as shown in Eq. (A.1).

For the standard k-ε model, R = 0 in Eq. (A.2). This term changes dynamically with the rate of strain of the turbulence, providing more accurate predictions for flows with rapid distortion [20]. This model was used in this study, because the effect of swirl on turbulence was considered, enhancing the accuracy for swirl flows.

To predict the spray break-up, we used the Kevin-Helmholtz (KH) Rayleigh–Taylor (RT) break-up model [21]. The KH-RT break-up model is often used for high pressure full-cone spray modeling. This model predicts spray break-up using KH instability [22] and RT instability [23]. The model constant was adjusted through validation with the results of the spray experiment.

To simulate the interaction between the droplet and wall, we used a wall film model developed by O'Rourke et al. [24]. Unlike other models, this model uses the film momentum equation in combination with the experimental results from Mundo et al. [25] in order to derive the spread-splash transition criterion [26]. The O'Rourke and Amsden wall film model considers film transport on complex surfaces, heating and vaporization of the film, separation and re-entrainment of the liquid film, and so on. [24].

To model evaporation, we used the Frossling correlation [27] as shown in Eq. (A.3).

In our simulation model, the base grid size is 4 mm. To increase the efficiency and stability of the simulation, using embedding, grid size near the wall was permanently set to 1 mm (scale 2). Also, that near the spark plug and in cylinder were set to 0.25 mm (scale 4) and 0.5 mm (scale 3), respectively, over the compression and expansion strokes. Furthermore, using adaptive mesh refinement (AMR), the region with a rapid velocity gradient over the entire time domain was locally refined into 1 mm (scale 2). The grid used in the simulation was shown in Fig. 7.

To evaluate grid independence, we compared the results of the reference mesh with these of the mesh refined permanently (AMR off) into 0.5 mm over in-cylinder or entire region, as shown in Fig. 7. For combustion modeling, we used the level set G-equation model [28] with the mechanism of Liu et al. [29]. Unlike the case when combustion is modeled only by the reaction mechanism, this model considers flame propagation by turbulence. The simulation domain can be divided into an unburned zone, a burned zone, and a flame zone using the parameter G. The G-equation model can trace turbulent flame by solving the Eq. (A.4) and Eq. (A.5).

2.3.2. Computational conditions

The engine simulation conditions are summarized in Table 4.

A six-stroke engine with the same specifications as the experiment was used for simulation. The engine speed was 1500 rpm. Since injection timing was sufficiently early, a pre-mixed condition was assumed for the PFI process. Iso-octane was used as the fuel for PFI. Also, the injection mass was adjusted so that the equivalence ratio was 1 under the same conditions as those in the experiment. Water was injected directly into the combustion chamber in the additional stroke. The water temperature was set to 90 °C. The injection pressure was set to 350 bar for atomization. The injection timing was set within a range of 60° before and after the TDC of re-compression. The injection mass of water was set to 10, 37.93, and 97.808 mg. The temperature of the cylinder wall was assumed to be constant. The simulation was conducted for a crank angle of 1080° from EVC (full exhaust) to EVC (full exhaust).

3. Results and discussion

3.1. Simulation model validation

The spray model was validated by comparing its results with the spray experiment results. The experimental and simulation conditions for model validation are summarized in Table 5.

First, the spray model was qualitatively validated by comparing the liquid spray images of the experiment and simulation. The images of the simulation and experiment are shown in Fig. 8. The simulation images followed those taken in the experiment well.

Next, the spray model was quantitatively validated by comparing the liquid spray penetration of the experiment and the simulation. In the experiment, the spray penetration was defined as the distance from the injector tip to the farthest point within the spray boundary. In the simulation, the spray penetration was defined as the distance from the nozzle to the point at which the accumulative mass fraction was 0.99. The spray penetrations of the experiment and the simulation are also shown in Fig. 8. The simulation results regarding spray penetration followed the experimental results well.

Before the simulation of the six-stroke engine, the combustion model

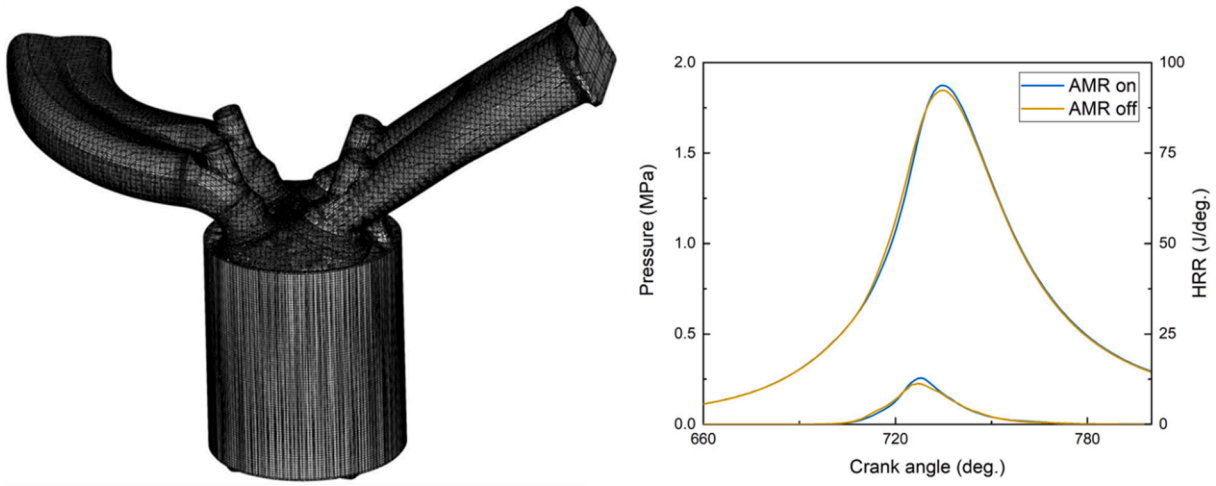

Fig. 7. Grid independence used in spray and combustion simulation.

Table 4
Engine simulation conditions.

Engine speed [rpm]		1500
4-stroke	**Fuel (PFI)**	Iso-Octane (C_8H_{18})
	Injection pressure	Pre-mixed
	Injection timing	
	Injection mass [mg]	14.144
Additional 2-Stroke	**Fuel (DI)**	Water (H_2O)
	Temperature of fuel [°C]	90
	Injection pressure [bar]	350
	Injection timing [° ATDC]	300 ~ 420
	Injection mass [mg]	10, 37.93, 97.808
	Spray pattern	Triangular shape

TDC: just before the combustion expansion stroke.

Table 5
Experimental conditions for spray model validation.

Injection pressure, P_{inj} [bar]	100, 200, 350
Injection duration [ms]	2
Ambient temperature [K]	300
Ambient pressure [bar]	1

was validated using the results of the four-stroke engine, since the six-stroke engine had the same processes as the existing four-stroke engine from full-exhaust to combustion expansion. The simulation results were compared with the experimental results based on the in-cylinder pressure and heat release rate. The comparison conditions are shown in Table 3. As shown in Fig. 9, the simulation results followed the experimental results well.

After the spray and combustion model validation, the simulation of the six-stroke engine was conducted for various partial exhaust duration, since the loss occurring in additional strokes was different depending on the amount of residual exhaust gas before the full-exhaust stroke. In this section, water direct injection was not included in the simulation for the partial exhaust duration optimization with a single operating point. We adjusted the partial exhaust duration by scaling the valve lift profile of the full-exhaust stroke. The valve lift profile corresponding to each duration is shown in Fig. 10. The profile of the CA 240° condition corresponds to the same profile as the full-exhaust stroke. The IMEP values for each condition are also shown in Fig. 10. As shown in Fig. 10, the IMEP was the highest under the condition that the partial exhaust duration was CA 180°. In accordance with the results, the partial exhaust duration was set to CA 180°, using the profile of the valve lift corresponding to this condition.

After partial exhaust duration optimization, the engine experiment was conducted after the actual cam was manufactured by reflecting the partial exhaust valve lift profile adopted earlier. Then, the six-stroke engine model was validated by comparing the results of the engine

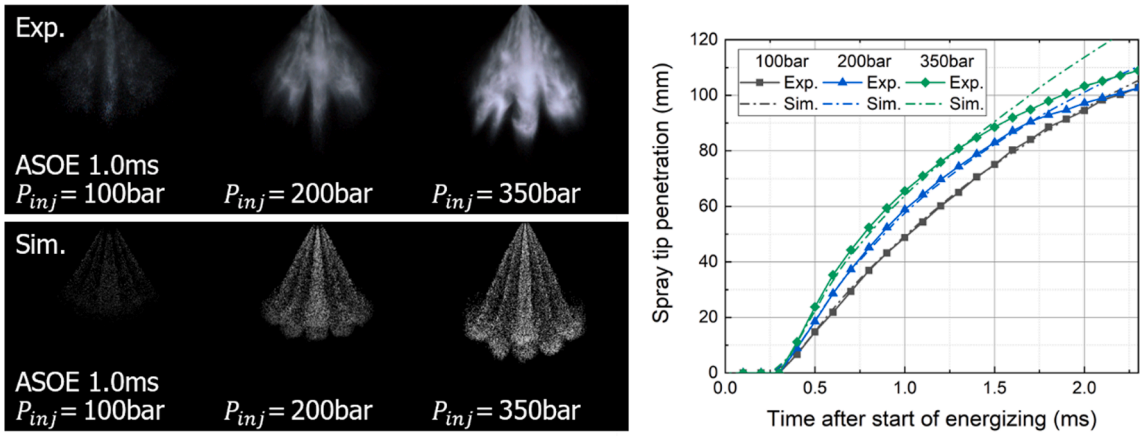

Fig. 8. Spray model validation with spray visualization and the spray penetration results in liquid phase.

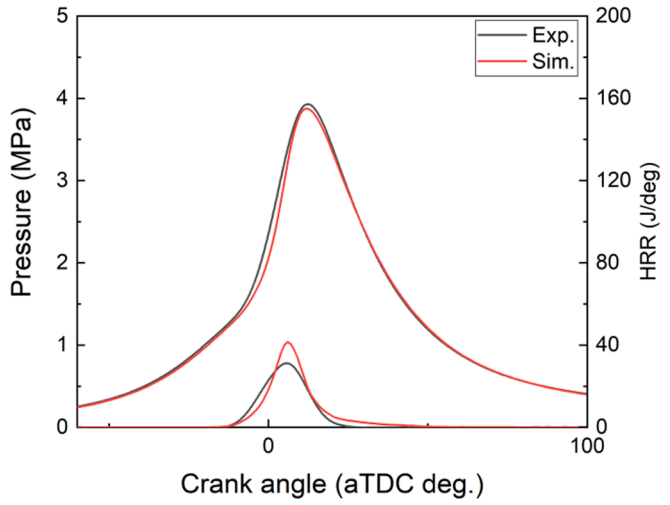

Fig. 9. Combustion model validation with the in-cylinder pressure and heat release rate.

experiment and simulation. This comparison was conducted for the six-stroke engine cases with and without water injection. The experimental and simulation conditions for the model validation are summarized in Table 6.

The result is shown in Fig. 11. As seen in Fig. 11, from combustion expansion stroke to additional strokes, the simulation results captured the experimental results well with respect to the in-cylinder pressure. To evaluate the effect of water injection, the IMEP values in the experiments and simulations were calculated.

As shown in Fig. 12, in the simulation, there was a slight increase in the IMEP from 5.48 bar to 5.489 bar when spraying at the TDC of re-compression, but it was still less than the four-stroke engine. However, in the experiment, the IMEP decreased by about 1 to 2% compared to the case without water injection, despite the injection at the TDC of re-compression. This difference occurred because, in the experiment, the cycle was repeated until the engine stabilized and then 99 cycles were repeated again for measurement. In other words, the cylinder wall was cooled due to continuous water injection[30]. Failure to bring the heat required for water to evaporate from the cylinder wall may cause a decrease in pressure, taking the heat from the mixture in the cylinder.

As shown in Fig. 13, in-cylinder pressure decreased after water injection because the cylinder wall was cooled down significantly and the evaporation of water was not carried out smoothly. The great challenge of the six-stroke engine was that it was difficult to control the wall temperature due to such cooling. If the engine load is increased to create a high-temperature environment and water is injected for cooling, the waste heat from high-temperature exhaust gases can be further utilized. Due to the limitations of the experimental system, it was difficult to implement such a high-load environment. However, since the purpose of this study was to evaluate the feasibility of the six-stroke engine using water injection, the simulation was conducted while maintaining the cylinder wall temperature at the same value as that used in combustion model validation for comparison with a four-stroke engine.

3.2. Six-stroke engine simulation with various injection timing

The simulation was conducted based on the previously set model. For more effective pressure increase, the water injection mass was increased to 37.93 mg. Since steam expansion occurred instead of combustion in the additional stroke, the evaporation rate of water was calculated instead of the heat release rate with the in-cylinder pressure. The evaporation rate was defined as follows:

$$(\textbf{Evaporationrate}) = \frac{\Delta m_{water,liquid}}{\Delta \theta}, \quad (1)$$

where $\Delta m_{water,liquid}$ is a change in mass of liquid water and $\Delta\theta$ is a change of the crank angle. After setting the injection timing within a range of 60° before and after TDC of the re-compression, the pressure and the evaporation rate were calculated. As shown in Fig. 14, when the water was injected early before the TDC of the re-compression, the pressure decreased considerably. Also, when the water was injected late, after the TDC of the re-compression, the pressure decreased slightly because water did not reach the wall and cooled the inside of the cylinder [31]. Only when the water was injected 340° and 360° after the TDC, such that the water evaporated near the TDC of the re-compression, the pressure increased. The results of IMEP were similar to the tendency of the in-cylinder pressure as shown in Fig. 14. When the water was injected 340° and 360° after the TDC, IMEP values were 5.52 bar and 5.53 bar, respectively, higher than the case without water injection. In

Table 6
Experimental conditions of water injection for the six-stroke engine model validation.

Injection pressure [bar]	350
Injection mass [mg]	10
Injection timing [° ATDC]	340 ~ 380

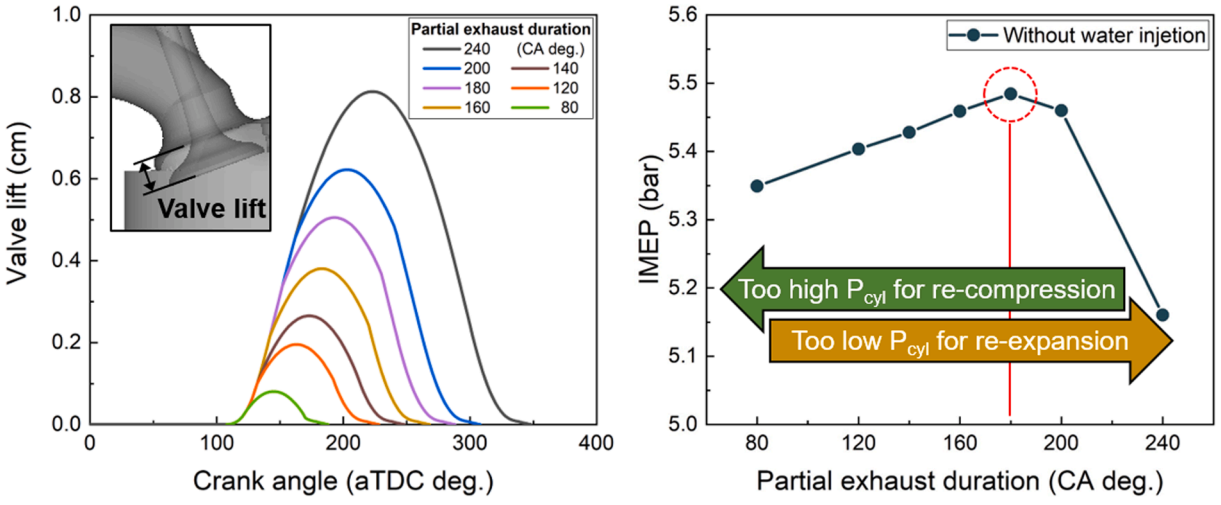

Fig. 10. Partial exhaust valve profiles and the IMEP of the six-stroke engine for various durations without water injection.

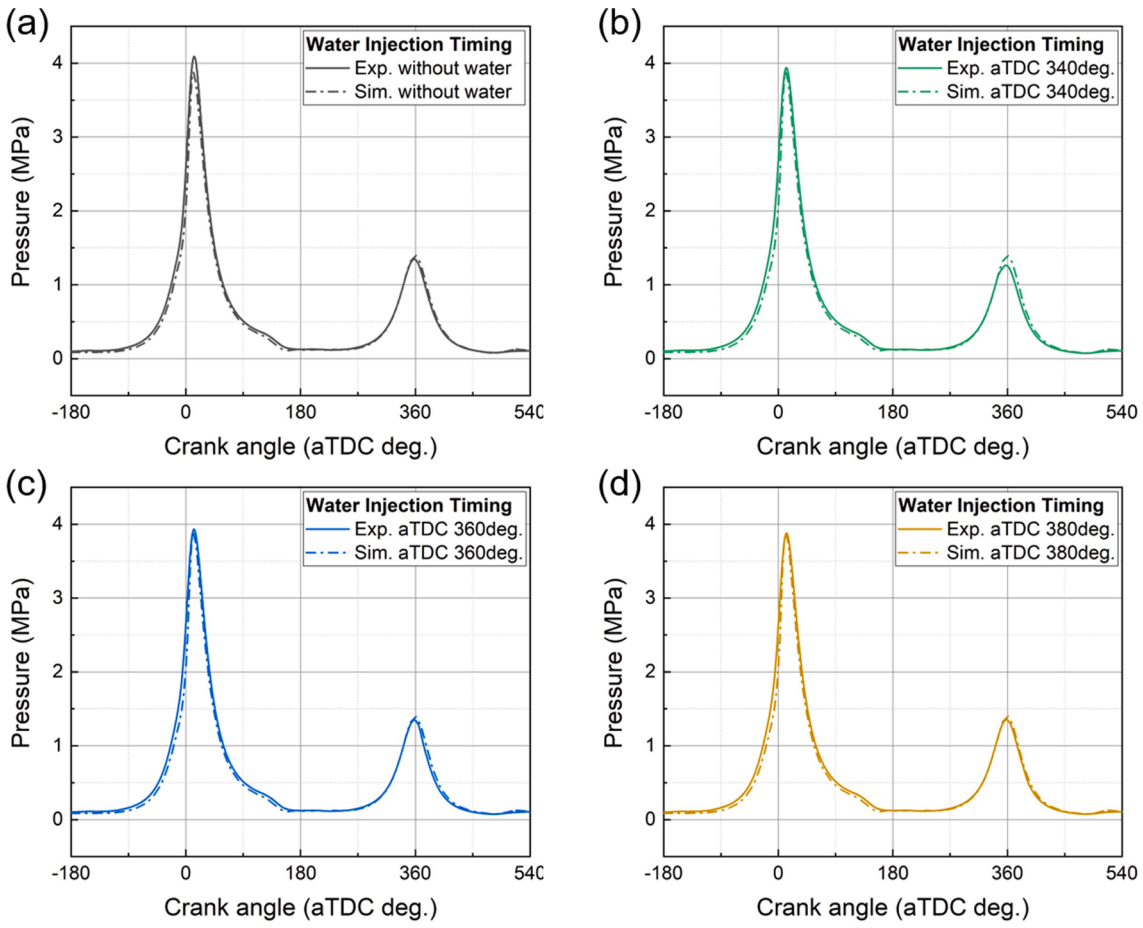

Fig. 11. Six-stroke engine model validation with in-cylinder pressure.

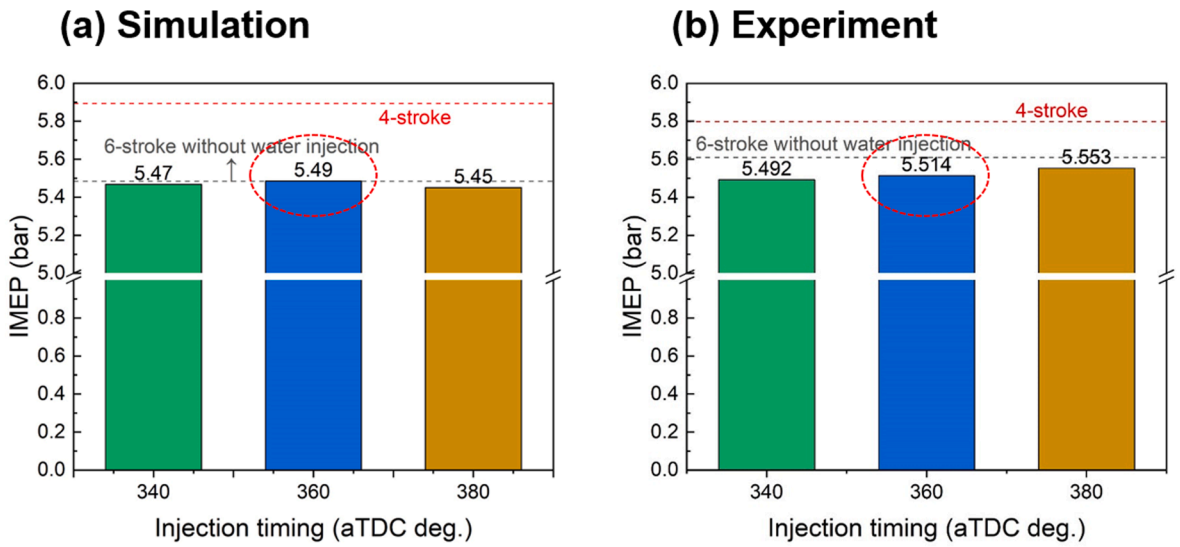

Fig. 12. IMEP values of the six-stroke engine in simulations and experiments.

the other cases, IMEP was lower than the case without water injection.

This result is related to the movement and evaporation of droplets. As shown in Fig. 15, the injected water moves through the mixture and hits the cylinder wall, repeating this process. In this process, the droplets absorb heat from the mixture while moving. Since the energy required for the evaporation of water is large, cooling is more dominant than steam expansion, making the pressure decrease. Meanwhile, when the thermal energy is taken from the wall, steam expansion may be performed without the in-cylinder pressure drop. As these two phenomena act in combination, the change in the pressure varies depending on the ratio of these phenomena. The higher the piston position, the shorter the distance to the cylinder wall, and the shorter the path of heat absorption. This can reduce the pressure drop and increase the rate of bringing in thermal energy from the wall. For this reason, when water was injected

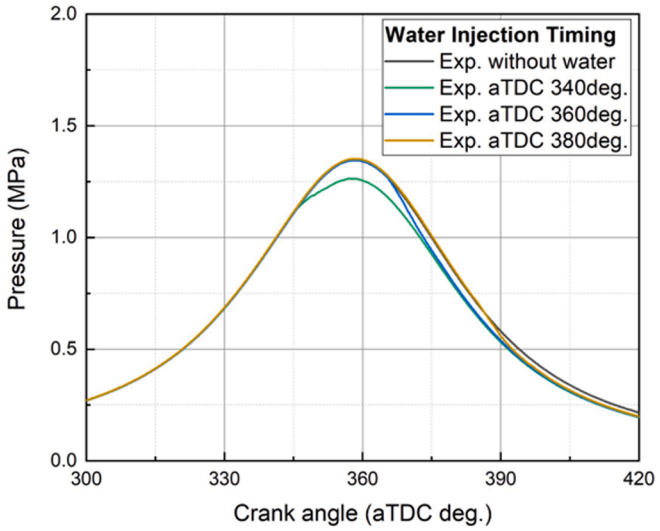

Fig. 13. In-cylinder pressure of the six-stroke engine in the experiment with 10 mg of water.

to evaporate near the TDC of the re-compression, the IMEP was higher than that of the case without water injection. However, even the highest IMEP was still lower than that of the four-stroke engine, because the pressure increased by only about 10% of the losses from the additional stroke. In the previous simulation, the effect of water injection was confirmed, but the IMEP was still lower than the results of the four-stroke engine. Therefore, the simulation was conducted with the amount of water increased to 97.81 mg to enhance its effect.

As shown in Fig. 16, when water is injected early before the TDC of the re-compression, the pressure drop was greatly reduced. This was due to the increased injection duration. As the injection mass increased, the injection duration was extended, and the section where the water evaporated spanned a range near the TDC of the re-compression. Thus, despite early injection, the IMEP was higher than that of the case without water injection as shown in Fig. 16. When injected at 340° after the TDC, the IMEP was the highest at 5.65 bar because this case had ideal evaporation timing near the TDC of the re-compression compared with the other cases. Combining this result with that of the previous simulation, it can be inferred that it is desirable to evaporate in the section from 360° after the TDC to 400° after the TDC. However, it still showed a lower IMEP compared to the four-stroke engine. To analyze this result, the results of the four-stroke engine and the six-stroke engine were compared using P-V diagram, as shown in Fig. 17. The water injection timing of these cases was 340° after TDC because this timing led to the highest IMEP in previous sections.

According to the previously suggested concept, positive work is performed in the re-compression and steam expansion strokes after the partial exhaust stroke. However, as shown in Fig. 17, negative work was performed in the results of this study. When water was injected, the pressure seemed to temporarily increase, but the pressure decreased through the subsequent process, resulting in negative additional work. In other words, the pressure needs to increase to values higher than those in these cases to obtain positive work.

3.3. Thermodynamic analysis of six-stroke engine

There are several parameters to consider in order to increase the in-cylinder pressure through water injection. The first thing to consider is the temperature of the water. Water compressed at high pressure is injected, expanded, and then evaporated through a heating process. Assuming an isenthalpic expansion process, the higher the temperature of the injected water, the less energy required to produce evaporation after expansion. This is shown in Fig. 18 using a T-v diagram of water.

As shown in Fig. 18, the high-temperature water can be located in the vapor dome on the T-v diagram after injection. When the pressure of the injected water drops to ambient pressure and is then positioned in the vapor dome after expansion, the energy required for evaporation is less than the latent heat of evaporation. Thus, it is possible to reduce the heat taken from the mixture. When heated to 523 K and 647 K, the quality (x) is 0.154 and 0.487, respectively, after expansion. However, even if half of the required energy is reduced, about 1000 kJ/kg of energy is required for evaporation based on an ambient pressure of 11 bar due to the large latent heat of water[32] which is about 10 times the latent heat of octane. In addition to the water temperature, the injection mass and wall evaporation ratio are also subject to consideration. The wall evaporation ratio is the ratio of energy taken from the wall to the energy required for evaporation. To understand the effects of these parameters, the pressure change in the cylinder after injection was thermodynamically calculated using energy conservation. The initial conditions were set from the average temperature and in-cylinder pressure obtained through combustion simulation of the six-stroke engine. The durations of injection and evaporation were neglected for simple analysis. The internal mixture was assumed to be air and an adiabatic process was assumed. Other assumptions are summarized in Table 7.

State 1 was defined as before water injection and state 2 was defined as after the point of water injection. By the steady-state assumption, the temperatures of water and air were the same in state 2. State 2 could be

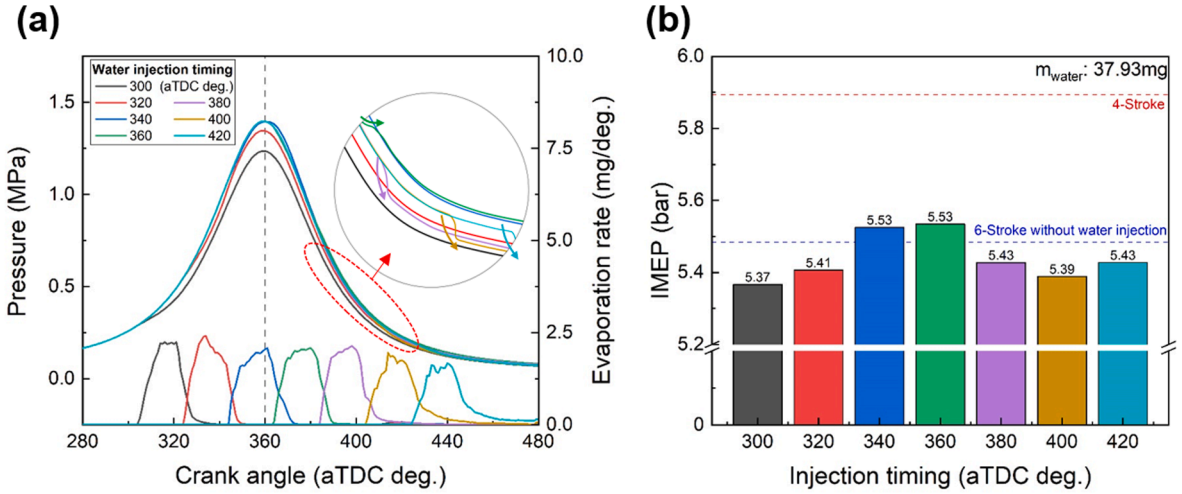

Fig. 14. In-cylinder pressure, evaporation rate of water and IMEP in the six-stroke engine with 37.93 mg of water.

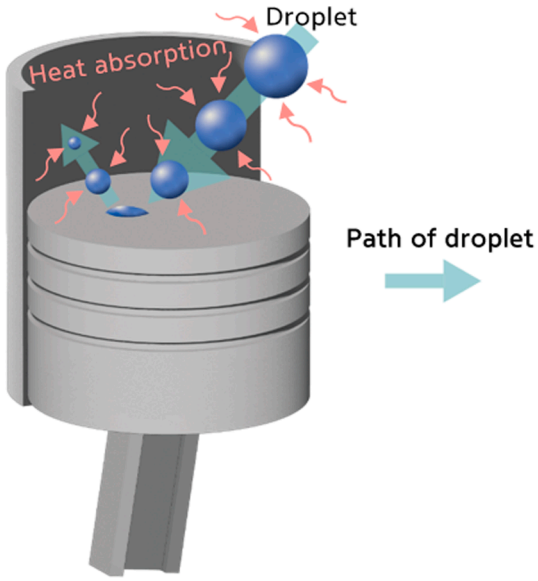

Fig. 15. Mechanism of heat absorption from the mixture in the cylinder.

determined by this temperature and Eq. (7). When state 2 was determined, the pressure change in the cylinder can be calculated by Eq. (8). In Fig. 19, the dotted line represents the part where the pressure change was zero, and the black area represents a condition in which water cannot evaporate perfectly.

$$|\Delta h_{air}| = |\Delta h_{water}| \quad (2)$$

when $T_{air,2} = T_{water,2}$.

$$\Delta P_{cyl} = \left(P_{air,2} + P_{water,2}\right) - P_{air,1} \quad (3)$$

As shown in Fig. 19, when water injection mass was increased, the effect on pressure change was different depending on the wall evaporation ratio. These differences were divided into left and right sides of the dotted line on the first contour. When this ratio was low, the pressure decreased as the mass increased. On the other hand, when this ratio was high, the pressure increased as the mass increased. Meanwhile, the effect of the water temperature was not critical compared to the wall evaporation ratio.

The simulation was conducted with an injection timing of ATDC 340° and injection mass of 97.81 mg while increasing the water temperature. As shown in Fig. 20, when increasing the water temperature,

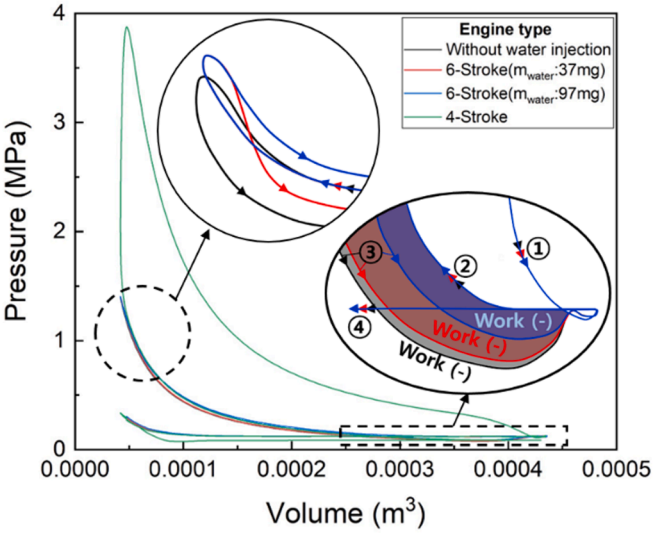

Fig. 17. P-V diagram: 4-stroke vs 6-stroke.

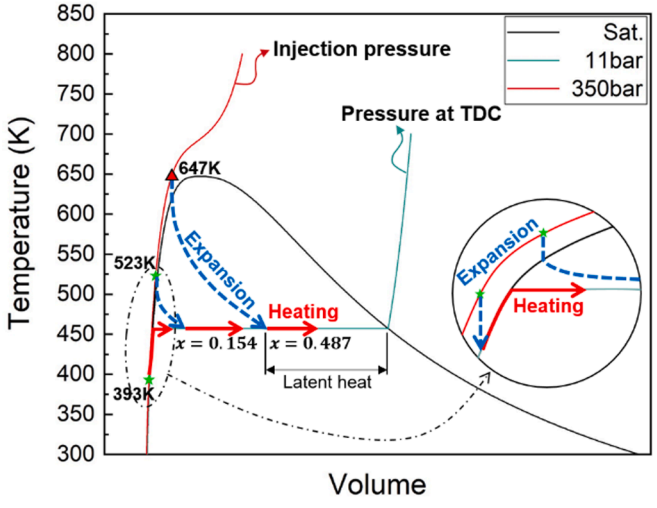

Fig. 18. Injection process on T-v diagram.

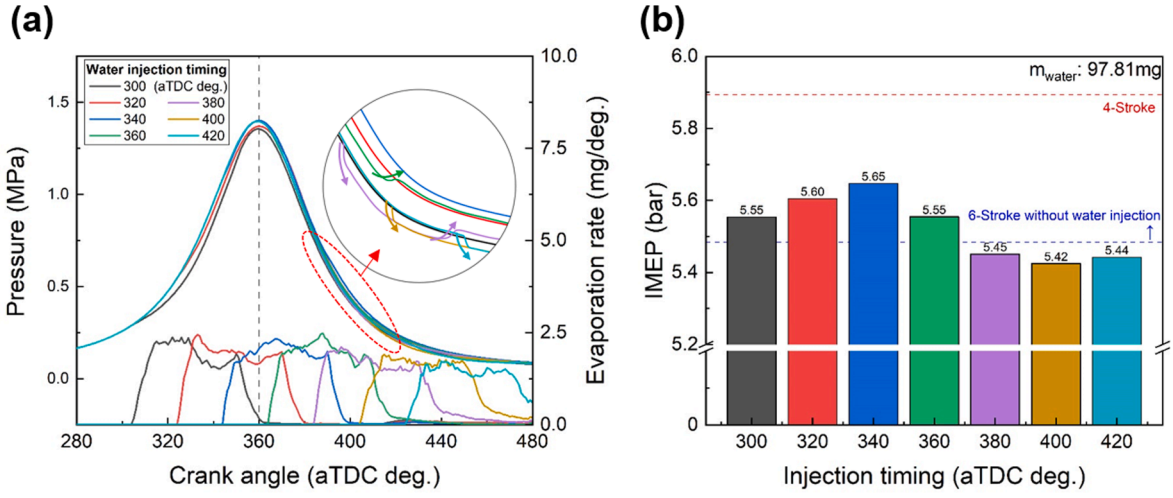

Fig. 16. In-cylinder pressure, evaporation rate of water and IMEP in the six-stroke engine with 97.81 mg of water.

Table 7
Initial conditions and assumptions for thermodynamic analysis.

Initial conditions	
Initial pressure ($P_{air,1}$)	11.7 bar
Initial temperature ($T_{air,1}$)	1467 K
Injection pressure ($P_{water,1}$)	350 bar
Assumptions	
- Isochoric at 340° after TDC	
- Adiabatic	
- Steady state, ideal gas	
- Air in cylinder	

the IMEP rose steadily, but it was still lower than that of the four-stroke engine. After all, the wall evaporation ratio is the key to increasing the pressure in the additional stroke. In other words, it can be inferred that the key is to bring as little heat energy as possible from the mixture. The core mechanism of the six-stroke engine cannot function properly unless it is not possible to bring heat from anywhere other than the mixture in the cylinder, for example from the wall or outside the cylinder.

The ideal condition to satisfy these requirements is steam injection. As shown in Fig. 21, it was confirmed through simulation that IMEP increased compared to the four-stroke engine when 97.81 mg of steam was injected with 20 bar of injection pressure. The pressure increased evidently during the additional stroke on the P-V diagram as shown in Fig. 21. If excessive cooling does not occur, the IMEP can increase due to an increase in mass. However, this is a very ideal case. It is difficult to obtain energy elsewhere for evaporation, and due to the latent heat of water, the mixture is inevitably cooled down making it difficult to realize this concept of six-stroke engine.

4. Conclusions

In this study, we conducted the six-stroke engine experiment and simulation to evaluate the feasibility and challenges of the six-stroke engine using water injection. After optimizing the exhaust valve lift profile through simulation, the experiment was performed with an actual cam manufactured by reflecting the results of simulations. The simulation model was validated through the experiment, and then it was analyzed whether it was possible to realize a six-stroke engine. The results are summarized as follows:

(1) When the actual six-stroke engine experiments were conducted, the cylinder wall was cooled by repeated water injection, making combustion and water evaporation unstable. By increasing the engine load and recovering cooling loss through water injection instead of coolant, evaporation of water can be more stable. Therefore, engine temperature control is essential and the

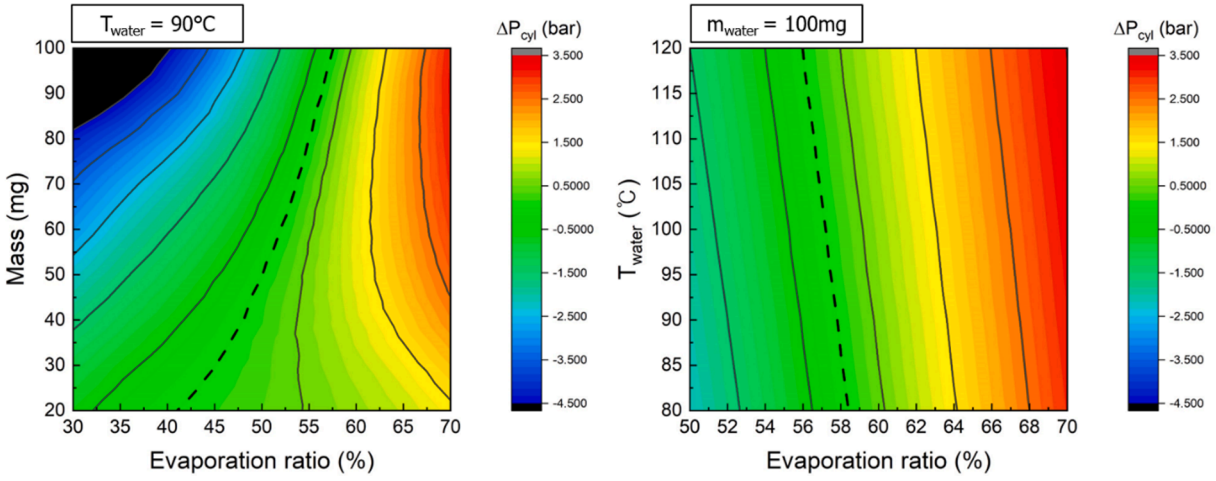

Fig. 19. Thermodynamic analysis of the pressure change in the cylinder using energy conservation.

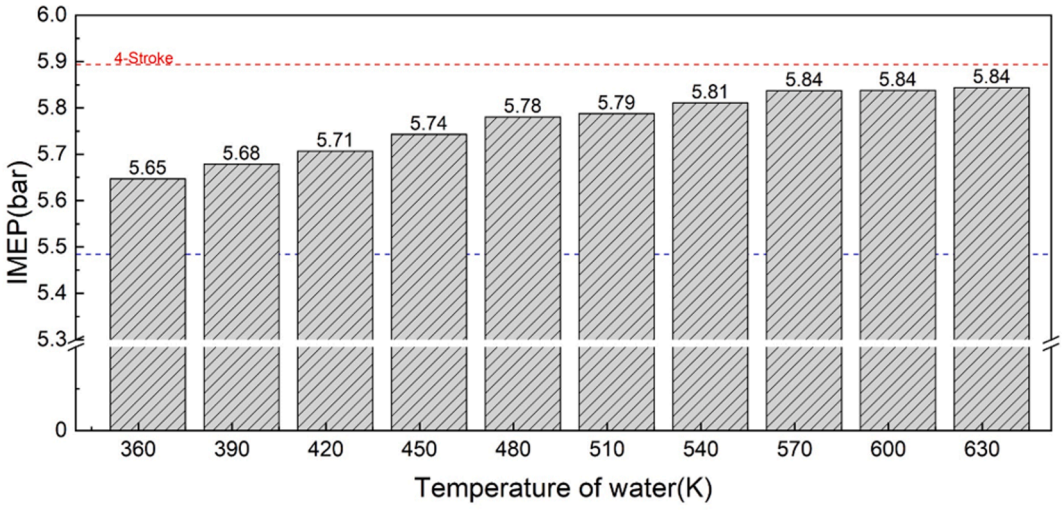

Fig. 20. IMEP in the six-stroke engine for various water temperatures.

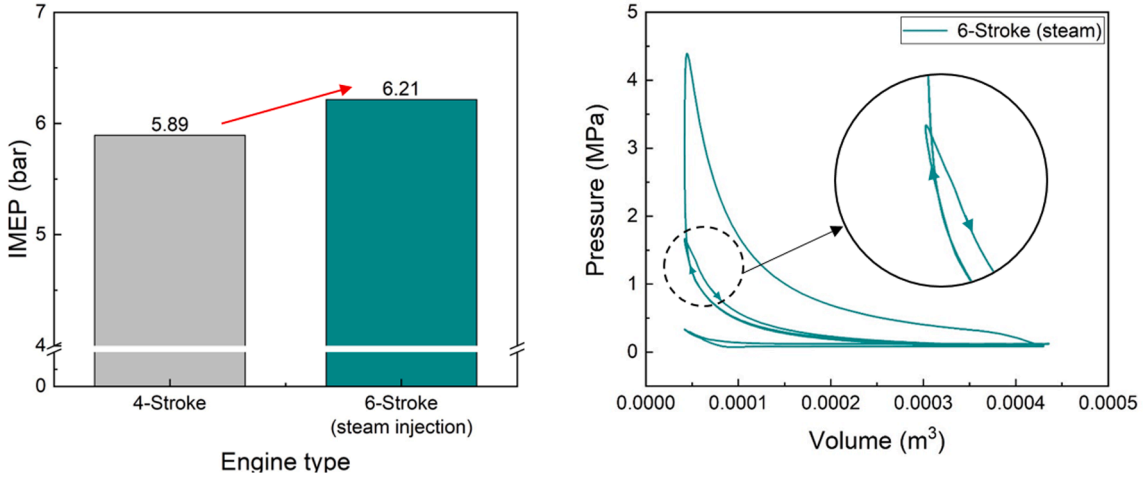

Fig. 21. IMEP and P-V diagram of the six-stroke engine with steam injection.

challenge for a six-stroke engine using water injection and that is the great challenge.

(2) In simulations, the additional stroke reduced IMEP by about 0.4 bar compared to that of the four-stroke engine, which was about 7% of the IMEP of the four-stroke engine. When 97.81 mg of water heated to 90 °C was injected, the IMEP was only recovered by 0.16 bar, which was about 40% of the loss.

(3) The wall evaporation ratio is more critical to the feasibility of the six-stroke engine than the mass and the water temperature. In other words, it is difficult to realize the six-stroke engine using water injection unless there is a method of obtaining a significant amount of heat energy from anywhere other than the mixture in the cylinder during injection, such as cooling loss. This is the second challenge for the realization of the six-stroke engine using water injection.

(4) If excessive cooling does not occur, the IMEP can increase due to an increase in mass, just as the IMEP increases when injecting steam. However, this is a very ideal case. It is difficult to obtain energy elsewhere for evaporation, and due to the latent heat of water, the mixture is inevitably cooled down making it difficult to realize this concept of six-stroke engine.

Declaration of Competing Interest

The authors declare that they have no known competing financial interests or personal relationships that could have appeared to influence the work reported in this paper.

Data availability

Data will be made available on request.

Acknowledgments

This work was supported by the National Research Foundation of Korea (NRF) grant funded by the Korea government(MSIT) (No. 2021R1A2C2011425).

Appendix A

$$\frac{\partial \rho \varepsilon}{\partial t}+\frac{\partial(\rho u_i \varepsilon)}{\partial x_i}=\frac{\partial}{\partial x_j}\left(\frac{\mu+\mu_t}{Pr_\varepsilon}\frac{\partial \varepsilon}{\partial x_j}\right)+C_{\varepsilon 3}\rho\varepsilon\frac{\partial u_i}{\partial x_i}+\left(C_{\varepsilon 1}\frac{\partial u_i}{\partial x_j}\tau_{ij}-C_{\varepsilon 2}\rho\varepsilon+C_s S_s\right)\frac{\varepsilon}{k}+S-\rho R, \tag{A.4}$$

where S is the user-defined source term, S_s is the source term that represents interactions with spray, and the $C_{\varepsilon i}$ terms are model constants that account for compression and expansion.

In Eq. (A.1),

$$R=\frac{C_\mu \eta^3(1-\eta/\eta_0)}{(1+\beta\eta^3)}\frac{\varepsilon^2}{k}, \tag{A.5}$$

where β is an adjustable constant and η is the ratio of the turbulence to mean strain.

$$\frac{dr_0}{dt}=-\frac{\alpha_{spray}\rho_g D}{2\rho_l r_0}B_d Sh_d, \tag{A.6}$$

where α_{spray} is the user-defined scaling factor for the mass transfer coefficient, D is the mass diffusivity of liquid vapor in air and Sh_d is the Sherwood number.

$$\frac{\partial \rho G}{\partial t}+\frac{\partial \rho u_i G}{\partial x_i}=-\rho D_t \kappa\left|\frac{\partial G}{\partial x_i}\right|+\rho_u S_t\left|\frac{\partial G}{\partial x_i}\right| \tag{A.7}$$

and

$$\frac{\partial \rho \overline{G}^{''2}}{\partial t}+\frac{\partial \rho u_i \overline{G}^{''2}}{\partial x_i}=\frac{\partial}{\partial x_i}\left(\rho D_t \frac{\partial \overline{G}^{''2}}{\partial x_i}\right)+2\rho D_t \frac{\partial \overline{G}}{\partial x_i}\frac{\partial \overline{G}}{\partial x_i}-c_s \rho \overline{G}^{''2}\frac{\varepsilon}{k}, \tag{A.8}$$

where s_t is the turbulent flame speed, ρ_u is the unburned density, k is the turbulent kinetic energy, ε is the turbulent dissipation, and c_s is a user-defined constant.

References

[1] N. Lam, M. Tuner, P. Tunestal, A. Andersson, S. Lundgren, B. Johansson, Double compression expansion engine concepts: a path to high efficiency, SAE Int. J. Engines 8 (4) (2015) 1562–1578.

[2] M. Yao, Z. Zheng, H. Liu, Progress and recent trends in homogeneous charge compression ignition (HCCI) engines, Prog. Energy Combust. Sci. 35 (2009) 398–437.

[3] M.A. Ceviz, A.K. Sen, A.K. Küleri, İ.V. Öner, Engine performance, exhaust emissions, and cyclic variations in a lean-burn SI engine fueled by gasoline–hydrogen blends, Appl. Therm. Eng. 36 (2012) 314–324.

[4] H. Hanabusa, T. Kondo, K. Hashimoto, H. Sono, M. Furutani, Study on homogeneous lean charge spark ignition combustion, in, SAE Technical Paper, 2013.

[5] Y. Yang, Y.S. Yu, M. Jeong, S. Park, Mixture formation enhancement in a direct-injection spark-ignition engine using horizontal injection, Fuel 326 (2022) 125121.

[6] S. Park, H.J. Kim, J.-T. Lee, Effects of various split injection strategies on combustion and emissions characteristics in a single-cylinder diesel engine, Appl. Therm. Eng. 140 (2018) 422–431.

[7] M. Costa, U. Sorge, S. Merola, A. Irimescu, M. La Villetta, V. Rocco, Split injection in a homogeneous stratified gasoline direct injection engine for high combustion efficiency and low pollutants emission, Energy 117 (2016) 405–415.

[8] C. Park, S. Kim, H. Kim, Y. Moriyoshi, Stratified lean combustion characteristics of a spray-guided combustion system in a gasoline direct injection engine, Energy 41 (2012) 401–407.

[9] H. Park, J. Lee, N. Jamsran, S. Oh, C. Kim, Y. Lee, K. Kang, Comparative assessment of stoichiometric and lean combustion modes in boosted spark-ignition engine fueled with syngas, Energ. Conver. Manage. 239 (2021) 114224.

[10] S. Furuhama, M. Takiguchi, K. Tomizawa, Effect of piston and piston ring designs on the piston friction forces in diesel engines, SAE Trans. (1981) 3018–3030.

[11] Z. Westerfield, P. Totaro, D. Kim, T. Tian, An experimental study of piston skirt roughness and profiles on piston friction using the floating liner engine, in, SAE Technical Paper, 2016.

[12] M. Kano, Super low friction of DLC applied to engine cam follower lubricated with ester-containing oil, Tribol. Int. 39 (2006) 1682–1685.

[13] M. Marian, T. Weikert, S. Tremmel, On friction reduction by surface modifications in the TEHL cam/tappet-contact-experimental and numerical studies, Coatings 9 (2019) 843.

[14] K.-P. Ha, D. Han, W.T. Kim, Development of continuously variable valve lift engine, in, SAE Technical Paper, 2010.

[15] K.-P. Ha, W.T. Kim, I. Ryu, Y. Son, Development of continuously variable valve duration (CVVD) engine, in: 25th Aachen colloquium automobile and engine technology, 2016.

[16] G. Fontana, E. Galloni, Variable valve timing for fuel economy improvement in a small spark-ignition engine, Appl. Energy 86 (2009) 96–105.

[17] J.C. Conklin, J.P. Szybist, A highly efficient six-stroke internal combustion engine cycle with water injection for in-cylinder exhaust heat recovery, Energy 35 (2010) 1658–1664.

[18] E. Arabaci, Y. İçingür, H. Solmaz, A. Uyumaz, E. Yilmaz, Experimental investigation of the effects of direct water injection parameters on engine performance in a six-stroke engine, Energ. Conver. Manage. 98 (2015) 89–97.

[19] V. Yakhot, S. Orszag, S. Thangam, T. Gatski, C. Speziale, Development of turbulence models for shear flows by a double expansion technique, Physics of Fluids A, Fluid Dyn. 4 (1992) 1510–1520.

[20] Z. Han, R.D. Reitz, Turbulence modeling of internal combustion engines using RNG κ-ε models, Combust. Sci. Technol. 106 (1995) 267–295.

[21] M.A. Patterson, R.D. Reitz, Modeling the effects of fuel spray characteristics on diesel engine combustion and emission, SAE Trans. (1998) 27–43.

[22] R.D. Reitz, Modeling atomization processes in high-pressure vaporizing sprays, Atomisation Spray Technol. 3 (1987) 309–337.

[23] G.I. Taylor, The instability of liquid surfaces when accelerated in a direction perpendicular to their planes. I, Proc. Royal Soc. Lond. Ser. A. Mathem. Phys. Sci., 201 (1950) 192–196.

[24] P.J. O'Rourke, A. Amsden, A spray/wall interaction submodel for the KIVA-3 wall film model, SAE Trans. (2000) 281–298.

[25] C. Mundo, M. Sommerfeld, C. Tropea, Droplet-wall collisions: experimental studies of the deformation and breakup process, Int. J. Multiph. Flow 21 (2) (1995) 151–173.

[26] C. Baumgarten, Mixture formation in internal combustion engines, Springer Science & Business Media, 2006.

[27] A.A. Amsden, P.J. O'Rourke, T.D. Butler, KIVA-II: A computer program for chemically reactive flows with sprays, in, Los Alamos National Lab. (LANL), Los Alamos, NM (United States), 1989.

[28] N. Peters (Ed.), Turbulent Combustion, Cambridge University Press, 2000.

[29] Y.-D. Liu, M. Jia, M.-Z. Xie, B. Pang, Enhancement on a skeletal kinetic model for primary reference fuel oxidation by using a semidecoupling methodology, Energy Fuel 26 (12) (2012) 7069–7083.

[30] M. Fratita, F. Popescu, J. Martins, F. Brito, T. Costa, Water injection as a way for pollution control, Energy Rep. 7 (2021) 543–549.

[31] W. Mingrui, N.T. Sa, R.F. Turkson, L. Jinping, G. Guanlun, Water injection for higher engine performance and lower emissions, J. Energy Inst. 90 (2017) 285–299.

[32] S. Zhu, B. Hu, S. Akehurst, C. Copeland, A. Lewis, H. Yuan, I. Kennedy, J. Bernards, C. Branney, A review of water injection applied on the internal combustion engine, Energ. Conver. Manage. 184 (2019) 139–158.